SSRG International Journal of Electrical and Electronics Engineering
ISSN: 2348-8379/ https://doi.org/10.14445/23488379/IJEEE-V13I8P109

Volume 13 Issue 8, 99-113, August 2026

Original Article

An Independent Validation and Analysis of a High-Efficiency Bidirectional DC Converter for Electric Vehicle Applications

Yogendra Kumar Sharma[1], Mohd. Suhaib Kidwai[2], Mohammed Aslam Husain[3], Akhtar Saleem Ansari[4]

[1]*ECD, Integral University, Lucknow (UP), India & CSD, AITD, Kanpur.*
[2]*ECD, Integral University, Lucknow (UP), India.*
[3]*Department of Electrical Engineering, BRSVBP Rajkiya Engineering College, Basti (UP), India.*
[4]*ECD, Integral University, Lucknow (UP), India & GP, Azamgarh (UP), India.*

[1]*Corresponding Author : yksharma@student.iul.ac.in*

Received: 01 May 2026 Revised: 08 July 2026 Accepted: 10 August 2026 Published: 25 August 2026

Abstract *- The increasing adoption of electric vehicles has led to an increased demand for high-efficiency, flexible bidirectional power conversion systems capable of providing two-way energy flow. This work presents an independent MATLAB/Simulink implementation and performance analysis of a high-efficiency bidirectional DC-DC converter for electric vehicle applications. The study investigates the converter's characteristics, including voltage conversion capability, semiconductor utilization factor, voltage stress on the switches, switching behavior, and efficiency under bidirectional operating conditions. A conventional PI-based closed-loop control is employed to ensure stable converter operation in both buck and boost modes. The performance of the converter is analysed through MATLAB/Simulink simulations in buck and boost modes to evaluate its response during vehicle charging and discharging operations. A 400 W system with a conversion range of 48 V to 200 V is modelled and simulated to examine its performance under key operating parameters such as power transfer capability, switching behaviour and efficiency. The results validate stable operation under varying operating conditions while achieving peak efficiency of 97.3% in buck mode and 96.9% in boost mode. The obtained results independently validate the performance characteristics of the investigated topology and provide insight into its suitability for use in electric vehicle and energy storage applications, where efficient energy exchange and reliable operation are essential.*

Keywords *- Modelling and simulation, Non-isolated topology, Voltage stress optimization, High voltage gain.*

1. Introduction

With the world's energy grid shifting toward cleaner and greener sources, the electrification of transportation has become a key pillar of global decarbonization efforts [1]. Vehicle to Grid (V2G) technology plays a key role by connecting Electric Vehicles (EVs) to the power network and transforming them from energy consumers to dynamic resources that support the grid [1, 2]. V2G allows EV batteries to act as distributed energy storage, charging when there is low demand or excess renewable generation and discharging there is peak demand [3]. This allows for improved grid stability through faster frequency response and spinning reserve, while also providing long-term benefits such as peak shaving and valley filling, which consequently enhance overall energy system efficiency and reliability [1, 4, 5].

One of the key enabling technologies of V2G and its counterpart (as illustrated in Figure 1), Grid to Vehicle (G2V) operation, is the bidirectional DC-DC converter [6]. This power electronic interface is responsible for bidirectional energy transfer between the EV battery and the high voltage DC bus or the grid, and has to be efficient, safe, and cost-effective. Since EV batteries typically operate at relatively low voltages, a high voltage gain, high efficiency converter is required to step up the battery voltage to the higher voltage levels required by charging infrastructure or the grid. The adjustable turns ratio of coupled-inductors makes coupled-inductor-based topologies particularly attractive because they can provide considerable high voltage gain [7, 8]. Yet they are usually limited by problems like leakage inductance, voltage overshoot on switches, and Electromagnetic Interference (EMI), especially without employing special snubber circuits [9-13].

Owing to their high voltage gain capability, coupled-inductor-based converters are the preferred option for industrial applications where safety and low Electromagnetic Interference (EMI) are significant concerns [14]. However, many existing bidirectional converter topologies satisfy only one or two practical requirements simultaneously. Some topologies provide a high voltage gain but require a large number of components and suffer from high capacitor voltage stress, whereas others have a simple structure but are confined to narrow voltage conversion ranges. For example, some conventional converters provide a step-down gains up to 0.5 and a step-up gains starting from 2 [15-19], whereas others provide narrower gain ranges, such as 0-1/3 and 3-∞ [8, 20-22] or 0-1/4 and 4-∞ [23]. These limited gain profiles reduce the flexibility and versatility of such converters for use with different EV voltage levels.

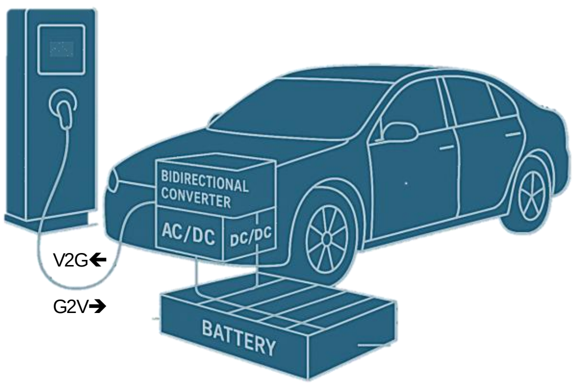

Fig. 1 Outline of EV charging setup

Additionally, some topologies create significant voltage stress across the switches, thereby increasing system cost and reducing reliability [24]. Quadratic-gain converters provide high gain, but they use more components and suffer from high capacitor stress [10, 12, 24]. Most of the existing designs lack a common problem of a shared ground, which leads to dv/dt issues, finally results in degrades overall system performance.

To address these challenges, the present study evaluates the performance of a high-gain converter architecture reported in [22] specifically designed for Electric Vehicle (EV) application with grid-to-vehicle integration capability. Additionally, the reported converter reduces the voltage stress across the switches and offers a wide high voltage gain range, with a simple and compact topology. Furthermore, the maximum switch voltage stress is limited to four times the high-voltage-side voltage; these features make the converter highly suitable for the dynamic and efficient EV grid interfacing in real situations.

In summary, the adopted converter topology offers several desirable characteristics for EV power conversion, including a wide and continuous voltage conversion range, common ground, reduced switch voltage stress and high semiconductor utilization. Motivated by these features, the present work presents an independent MATLAB/Simulink implementation of reported converter for a 400-W,48 V/200 V voltage configuration. The converter is analyzed under Continuous Conduction Mode (CCM) using a conventional PI-based closed-loop controller. The study investigates the converter's steady state and dynamic performance in both buck and boost operating modes, with emphasis on voltage conversion capability, switching behavior, power transfer characteristics and conversion efficiency.

This paper is organized as follows: Section 2 is about the literature review of relevant bidirectional DC-DC converters and identifies the research gap. Section 3 presents the circuit diagram, its operating principles and corresponding governing equations. Section 4 describes the converter modeling and simulation using MATLAB/Simulink. Section 5 presents an in-depth comparison with state-of-the-art converter topologies. Finally, Section 6 concludes the research with future directions.

Research Gap and Novelty: Although several bidirectional DC-DC converter topologies have been investigated for EV applications, previous studies have mainly focused on converter development, analytical investigations and advanced control techniques. However, further evaluation of reported converter topologies under diverse operating conditions and system specifications remains necessary for implementation and suitability for EV charging applications. Accordingly, the present work addresses this need through an independent MATLAB/Simulink implementation and detailed performance evaluation of a reported high-gain bidirectional converter topology under different operating conditions and system specifications.

In particular, there remains a need to investigate the behavior of established converter topologies at different power ratings and voltage levels using widely adopted simulation-based approaches to facilitate system-level analysis, performance verification, and future controller development.

To address this gap, the present work adopts the high-gain bidirectional DC/DC converter topology and presents its independent MATLAB/Simulink implementation for a 400-W EV charging application with a 48 V/200 V operating configuration. While [22] investigated both CCM and DCM operation using a dead-beat controller, the present study focuses on CCM operation and employs a conventional PI-based closed-loop controller. The PI controller was selected due to its simple structure, ease of implementation and widespread use on practical power electronic applications. Although deadbeat control can provide faster transient response, it generally needs accurate modeling and higher computational complexity. Therefore, the adopted control strategy provides a balance between implementation simplicity and dynamic performance for the considered EV application. The extension of the analysis to DCM operation is identified as a potential direction for future work.

The work further provides a comprehensive performance assessment of the converter in both buck and boost modes, including voltage conversion characteristics, switching behavior, power transfer capability and conversion efficiency under the selected operating conditions.

These investigations provide an independent validation of the converter performance and enable an evaluation comparative understanding of the adopted converter topology under different operating specifications. The obtained results provide useful information to establish a simulation framework for future studies involving advanced control strategies and practical hardware implementation of bidirectional EV charging systems.

2. Literature Review

A wide variety of bidirectional DC-DC converter topologies have been reported in the literature for electric-vehicle and energy-storage applications. Broadly, these can be classified into isolated and non-isolated structures. Isolated topologies, such as the Dual Active Bridge (DAB) and CLLC resonant converters, provide galvanic isolation together with bidirectional power flow and are widely preferred for high-power on-board chargers; their capability to achieve soft switching contributes to high efficiency over a broad operating range. However, the use of high frequency transformers and a relatively large number of switches, which increases size, cost, and control complexity making these topologies less attractive for compact and medium power applications.

Non-isolated topologies are attractive for compact and cost-sensitive applications. Conventional cascaded and interleaved buck/boost converters provide a simple structure, but provide a limited voltage conversion ratio. Coupled inductor-based converters can achieve a high voltage gain through an adjustable turn's ratio, but they are affected by leakage-inductance effects, voltage overshoot across the switches, and electromagnetic interference unless additional snubber circuits are employed.

To overcome this limitation, several enhanced non-isolated topologies have been developed. Coupled-inductor converter offers improved voltage-gain capability through magnetic coupling.

However, their performance is influenced by leakage inductance, which can cause voltage overshoots across the semiconductor devices and increase electromagnetic interference; consequently converter needs auxiliary clamp or snubber circuits to reduce these effects. Switched-capacitor and switched-quasi-Z-source converters have been developed to extend the gain range, however many reported configurations operate effectively over a limited voltage gain regulation only, which reduces their suitability for applications requiring continuous wide range voltage regulation [22]. Quadratic-gain converters offer a very high gain capability but at the expense of an increased component count and high capacitor stress, while several reported topologies lack a common ground, leading to dv/dt problems that degrade overall performance.

A consolidated comparison of these representative topologies, including their voltage-gain expressions, gain ranges, power levels, switching frequencies, and reported efficiencies, is presented in Table 2, and a comparison of their circuit complexity and application suitability is given in Table 3. The literature survey indicates that existing bidirectional converter topologies offer distinct advantages on intended application while trade-offs among a wide continuous voltage range, low semiconductor stress, high efficiency and circuit complexity. In view of these observations, present work focuses on independent validation and detailed evaluation of reported converter to examines its performance.

3. Circuit diagram of the converter and related operational analysis

3.1. Overview of the Converter Design

Figure 2 illustrates the bidirectional DC/DC Converter topology adopted in study. The converter serves as an efficient power conversion interface between the electric vehicle's battery (Low voltage side, denoted as V_{LV}) and a high voltage side DC link or storage unit (high voltage side denoted as V_{HV}) [22]. Consequently, the converter supports both Grid-to-Vehicle (G2V) charging and Vehicle-to-Grid (V2G) discharging. The main components of the converter circuit are mentioned as follows:

- 5 switches: S_{u1}, S_{u2}, S_{d1}, S_{d2}, and S_{d3}
- 4 capacitors: C_1, C_2, C_3, and C_4
- 2 inductors: L_1 and L_2

These switches work together to control the direction and amount of power transfer. Their body diodes also conduct current during the switching time (T_s). In a practical setup, the converter is connected to the AC grid through a full bridge inverter of single-phase. This allows power to flow in both directions, enabling V2G/G2V integration.

Such bidirectional operation allows battery charging as well as the return of stored battery energy to the grid during peak demand. Consequently, overall grid flexibility is improved while energy utilization is managed more effectively. Depending on the operating mode, different switch groups are employed for synchronous rectification. During the step-up operation, this function is carried out by switches. S_{u1} and S_{u2} , whereas during step-down operation, switches S_{d1}, S_{d2}, and S_{d3} perform same function.

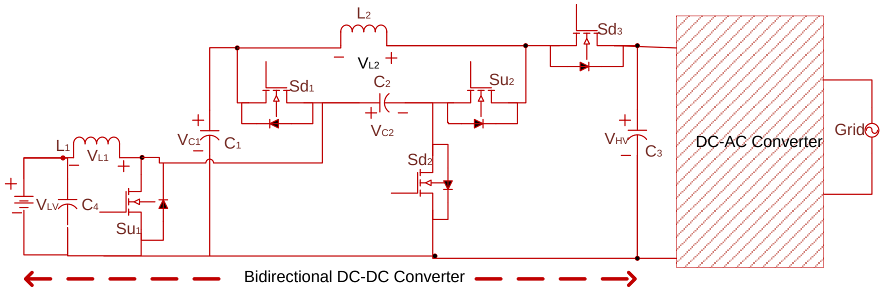

Fig. 2 Presented bidirectional DC-DC converter connected to grid through Inverter

3.2. Step-Up (Boost) Mode Operation

Under boost mode operation, power flows from the EV battery (V_{LV}) to the high-voltage side (V_{HV}). Two operating cases are defined under Continuous Conduction Mode (CCM):

Case 1: $0 \leq t \leq T_{on}$

As depicted in Figure 3, switches S_{u1} and S_{u2} are in the conducting state, whereas switches S_{d1}, S_{d2}, and S_{d3} stay inactive.

During this period:

- The inductor L_1 charged by the EV battery.
- Capacitors C_1 and C_2 discharge their stored energy into the inductor L_2.

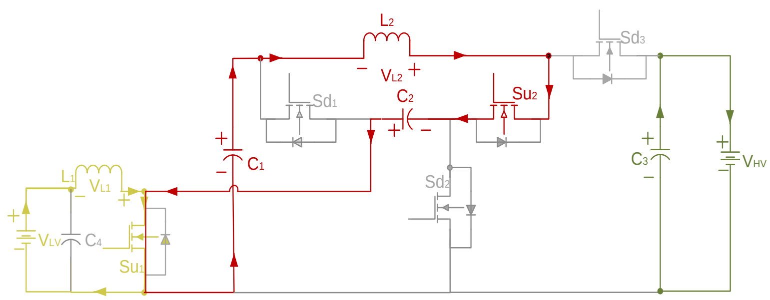

Fig. 3 Current flow direction in step-up/boost mode when Switches Su$_1$ and Su$_2$ in ON state for equivalent circuit

The voltages are represented by following equations:

$$v_{L1} = L_1 \frac{di_{L1}}{dt} = V_{LV} \quad (1)$$

$$v_{L2} = L_2 \frac{di_{L2}}{dt} = v_{C1} + v_{C2} \quad (2)$$

Case 2: $T_{on} \leq t \leq T_s$

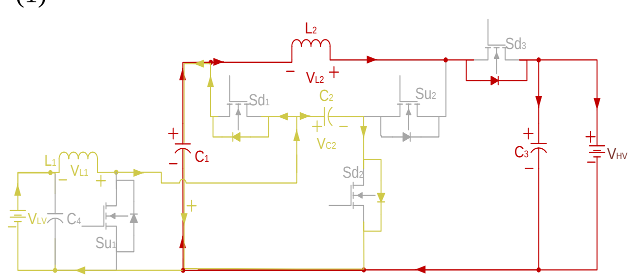

Fig. 4 Corresponding current flow direction in the step-down/buck mode when Switches Su1 and Su2 are in OFF state. body diodes of switches Sd$_1$, Sd$_2$ and Sd$_3$ conducts

As depicted in Figure 4, switches S_{u1} and S_{u2} are in the non-conducting state, whereas the body diodes of switches S_{d1}, S_{d2}, and S_{d3} remain in the conducting state.

Here:

- The inductor L_1 transfers its stored energy to capacitor C_2.
- The inductor L_2 transfers energy to the high-voltage terminal V_{HV} .

The governing equations are given in (3) and (4).

$$v_{L1} = -v_{C1} + V_{LV} = -v_{C2} + V_{LV} = L_1 \frac{di_{L1}}{dt} \quad (3)$$

$$v_{L2} = +v_{C1} - V_{HV} = +v_{C2} + V_{HV} = L_2 \frac{di_{L2}}{dt} \quad (4)$$

From (3) & (4), it can be seen that $v_{C2} = v_{C1}$. Applying volt-second balance, the following equations are obtained:

$$(V_{LV})D + (V_{LV} - V_{C1})(1 - D) = 0 \quad (5)$$

$$(V_{C1} + V_{C2})D + (-V_{HV} + V_{C1})(1 - D) = 0 \quad (6)$$

Solving (5) and (6) gives the following equation:

$$V_{C1} = V_{C2} = \frac{V_{LV}}{(1-D)} \quad (7)$$

Thus, the voltage boost ratio for step-up mode for continuous conduction operation is given in Equation (8).

$$\frac{V_{HV}}{V_{LV}} = M_{boost} = \frac{D+1}{(1-D)^2} \quad (8)$$

3.3. Step-Down (Buck) Mode Operation

In step-down mode, power is transferred from the high-voltage side (V_{HV}) to the EV battery (V_{LV}). This operation also consists of two cases under CCM:

Case A: $0 \le t \le T_{on}$

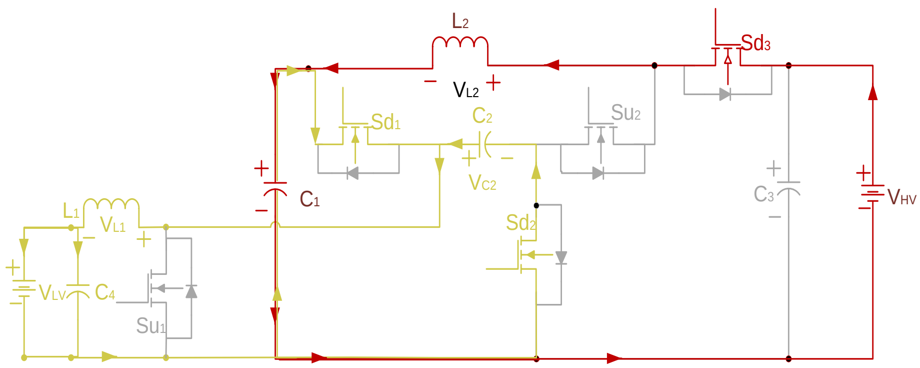

Fig. 5 Current flow direction in the step-down/Buck mode when Switches Sd$_1$, Sd$_2$ and Sd$_3$ are in ON state

As illustrated in Figure 5, switches S_{d1}, S_{d2}, and S_{d3} are in the conducting state, whereas switches S_{u1} and S_{u2} are remain in the OFF state.

Here:

- The inductor L_2 is charged by a high-voltage source V_{HV} and capacitor C_1.
- The inductor L_1 receives energy from a capacitor C_2.

The equations are given in (9) and (10).

$$L_1 \frac{di_{L1}}{dt} = v_{L1} = +v_{C1} - V_{LV} = +v_{C2} - V_{LV} \quad (9)$$

$$L_2 \frac{di_{L2}}{dt} = v_{L2} = -v_{C1} + V_{HV} = -v_{C2} + V_{HV} \quad (10)$$

From Equations (9) and (10), it can be observed that $v_{C2} = v_{C1}$

Case B: $T_{on} \le t \le T_s$

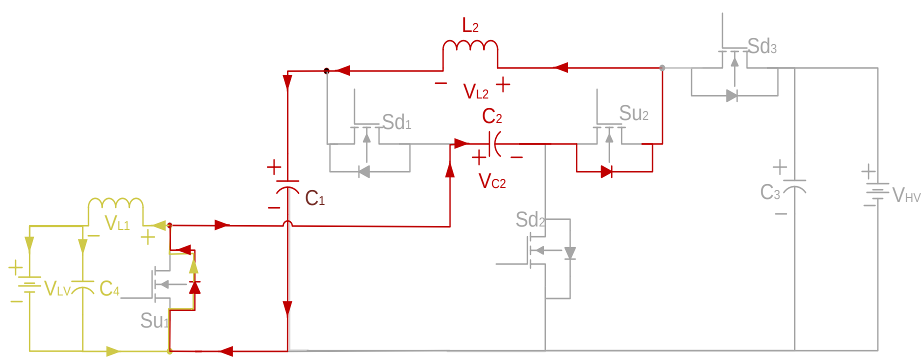

Fig. 6 Corresponding current flow direction in the step-down/buck mode when Switches Sd$_1$ and Sd$_2$ are in OFF state and the body diodes of switches Su$_1$ and Su$_2$ conduct

Similarly, as illustrated in Figure 6, switches S_{d1}, S_{d2}, and S_{d3} are in the non-conducting state, whereas the body diodes conduct for switches S_{u1} and S_{u2}.

During this interval:

- The stored energy of the inductor L_1 is shifted to the EV battery.

- Similarly, the stored energy of the inductor L_2 is shifted to the capacitors C_1 and C_2.

The corresponding equations are given in (11) & (12):

$$L_1 \frac{di_{L1}}{dt} = v_{L1} = -V_{LV} \tag{11}$$

$$L_2 \frac{di_{L2}}{dt} = v_{L2} = -v_{C1} - v_{C2} \tag{12}$$

By applying volt-second balance, the following equations can be obtained:

$$(-V_{LV})(1-D) + (V_{C1} - V_{LV})(D) = 0 \tag{13}$$

$$(-V_{C2} - V_{C1})(1-D) + (V_{HV} - V_{C1})(D) = 0 \tag{14}$$

In this expression, parameter D represents the duty cycle. By solving the above equations, the following expression is obtained:

$$V_{C2} = V_{C1} = \frac{V_{LV}}{D} \tag{15}$$

Based on Equations (14) and (15), the voltage gain of the presented converter during buck-mode operation in Continuous Current Mode (CCM) can be determined using Equation (16).

$$M_{buck} = \frac{V_{LV}}{V_{HV}} = \frac{D^2}{2-D} \tag{16}$$

The corresponding waveforms for continuous conduction mode are shown in Figure 7.

3.4. Duty Cycle Formulation

Using the voltage gain expressions from Equations (8) and (16), the duty cycles associated with continuous conduction mode for step-up/boost and the step-down/buck operations are obtained as follows:

- For boost mode, the duty cycle is given in Equation (17) as follows:

$$D_{Boost} = \frac{V_{LV} + 2V_{HV} - \sqrt{8V_{LV}V_{HV} + V_{LV}^2}}{2V_{HV}} \tag{17}$$

- For buck mode, the duty cycle is given in Equation (18) as follows:

$$D_{Buck} = \frac{-V_{LV} + \sqrt{8V_{HV}V_{LV} + V_{LV}^2}}{2V_{HV}} \tag{18}$$

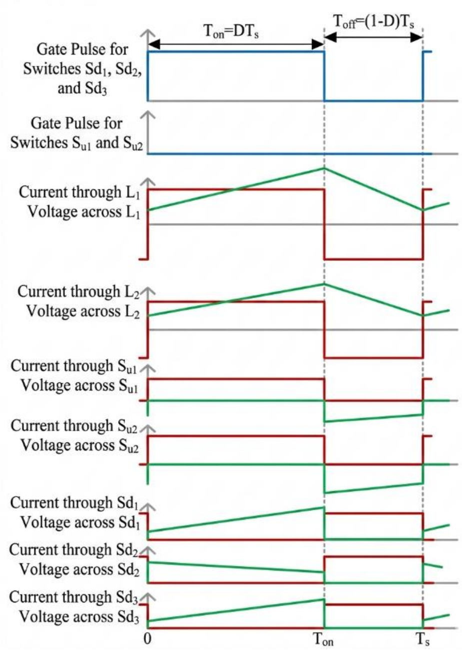

Fig. 7 Time-based waveforms during buck (step-down) mode for continuous conduction operation

These expressions enable precise control of voltage conversion in both operating modes, which is critical for reliable EV charging and discharging in practical applications. In this work, analytical duty-cycle control is employed to verify the fundamental operational characteristics and voltage conversion behavior of the topology. Since the primary goal of this study is the evaluation of topology and its performance analysis, advanced closed-loop (or intelligent) control strategies were not incorporated at this stage. However, future studies could utilize additional techniques such as PI-controlled feedback systems, model predictive control, fuzzy logic control, and/or optimization-assisted controllers to potentially improve dynamic response and robustness.

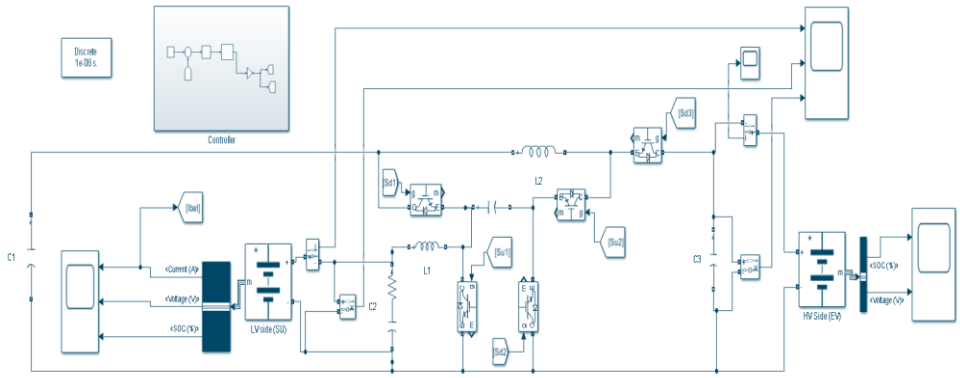

Fig. 8 MATLAB/Simulink model of the presented bidirectional converter

4. Modeling and Analysis of the Bidirectional Converter using MATLAB/Simulink

A systematic model of the presented bidirectional DC-DC converter has been implemented with Simulink/MATLAB to test its functionality and performance. The complete setup of the modelled converter circuit is shown in Figure 8. This model accurately represents how this DC-DC converter will behave when charging or discharging power in either mode, i.e., step-up (boost) or step-down (buck) configurations. The key parameters used in simulations are listed in Table 1 and are based on a typical EV energy transfer scenario. In particular, the converter interfaces between the LV battery (48 V) and HV/storage unit (200 V) for energy exchange in electric vehicles.

Table 1. Simulation parameters for the presented converter

Parameters	Values
Rated Output Power (W)	400W
Switching frequency (f_s)	50kHz
LV and HV side voltages (V_{LV}, V_{HV}):	48V and 200V
Inductors L_1, and L_2	0.39mH, 1.0mH
Capacitors C_1, C_2, C_3 and C_4:	25µF,25µF, 1000µF, 1000µF

A discrete-time MATLAB/Simulink model was implemented to simulate the presented topology and employed a discrete-time solver with a fixed step-size of 1e-6 s to accurately simulate the switching dynamics associated with the chosen 50 kHz switching frequency. Nominal initial values of capacitor voltages and battery State-of-Charge (SoC), representative of typical EV operating conditions, were established.

4.1. Step-Up (Boost) Mode Operation

The next three figures show the converter's operation in boost mode. In this mode, the energy is transferred from low voltage battery (EV side) to high voltage (Storage Unit (SU) side) battery. In Figure 9, the low-side battery current and SOC both decrease, indicating the battery on low voltage side is discharging. As a result, in Figure 10, energy is transferred to the high voltage side battery, as indicated by the increasing voltage and SOC values. Finally, Figure 11 provides insight into the switching pattern of the converter. The switching operation of the converter is analysed as follows. When switch Su_1 is ON, switch S_{d1} is OFF. and when Su_1 is turned OFF, the current flows through the body diode of $S_{d1,}$ confirming that the converter is performing in boost mode.

4.2. Step-Down (Buck) Mode Operation

The converter transfers energy from the high-voltage source (HV or SU) to the low-voltage battery (LV or EV). In Figure 12, it is indicated that the low-voltage battery is being charged as demonstrated by an increase in SOC and the positive charge flow. In Figure 13, it is observed that the high voltage source SOC has decreased, indicating that the SU is providing energy to the converter. Figure 14 presents the switching pattern during buck-mod configuration. When S_{d1} is active, S_{u1} remains OFF, and during the OFF duration, the current flows through the body diode of $S_{u1,}$ confirming the buck operation. This converter ensures a seamless transition between charging and discharging in bidirectional operation, making the presented converter highly suitable for practical electric vehicle charging /discharging applications.

5. Results and Discussion

The comparative analysis of key bidirectional DC converters with respect to the presented converter is shown in Table 2. The comparison emphasizes the important performance parameters against various existing converter topologies. The performance variation between the present implementation and the reported converters is influenced by several factors, including converter topology, operating conditions, power rating, voltage conversion range, control strategy, and component selection. Therefore, a direct comparison of performance parameters should be considered carefully due to the differences in design specifications and operating conditions. The results obtained in this work demonstrate the capability of the adopted topology for efficient bidirectional operation under the selected 400-W, 48-V/200-V configuration and provide an independent evaluation of its performance characteristics.

Table 2. Comparison of main bidirectional DC-DC converters

Topology Reference	Components Used C: Capacitor, L: Inductor, S: Switch, D: Diode	Voltage Gain Expression Buck (↓)	Voltage Gain Expression Boost (↑)	Voltage Gain Range Buck-Boost Range	Power Output (W)	Switching Frequency (kHz)	Maximum Efficiency Buck, Boost
[10]	3C, 2L, 4S	D^2	$1 / (1 - D)^2$	0 to ∞	100	50	93.7%, 95.5%
[25]	3C, 1L, 4S	D	1 / (1 - D)	0 to ∞	1000	50	< 97%
[12]	3C, 2L, 4S	D^2	$1 / (1 - D)^2$	0 to ∞	160	30	95.0%, 96.5%
[26]	2C, 2L, 3S	D/ (2 - D)	(1+D) / (1-D)	0 to ∞	200	50	96.7%, 96.2%
[8]	6C, 3L, 8S	D / 3	3 / (1 - D)	0-1/3 / 3-∞	800	20	95.9%, 95.8%
[19]	4C, 1L, 4S	D / 2	2 / (1 - D)	0-0.5 / 2-∞	300	20	94.45%, 94.39%
[16]	4C, 1L, 4S	D / 2	2 / (1 - D)	0-0.5 / 2-∞	140	70	96.3%, 97.5%
[18]	4C, 2L, 4S	D / 2	2 / (1 - D)	0-0.5 / 2-∞	3000	50	97.6%, 97.4%
[17]	6C, 2L, 5S	D / (3 - D)	(2 + D) / (1 - D)	0-0.5 / 2-∞	400	20	94.41%, 94.09%
[24]	3C, 2L, 2D, 4S	D^2	$1 / (1 - D)^2$	0 to ∞	200	15	88.7%, 83.2%
[20]	5C, 2L, 6S	$D^2 / (2 + D)$	$(3 - D) / (1 - D)^2$	0-1/3 to 3-∞	2000	100	97.4%, 97.2%
[22]	4C, 2L, 5S	$D^2 / (2 - D)$	$(1 + D) / (1 - D)^2$	0 to ∞	500	50	97.2%, 96.8%
Presented	4C, 2L 5S	$D^2 / (2 - D)$	$(1 + D) / (1 - D)^2$	0 to ∞	400	50	97.3%, 96.9%

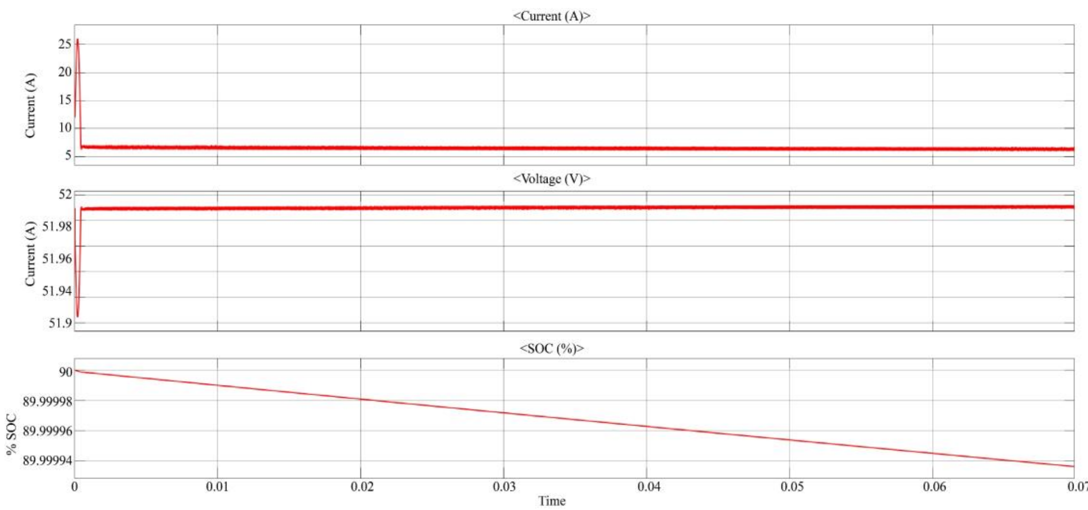

Fig. 9 Voltage, current and state of charge during step up/ boost mode in Low-voltage (EV side) battery side

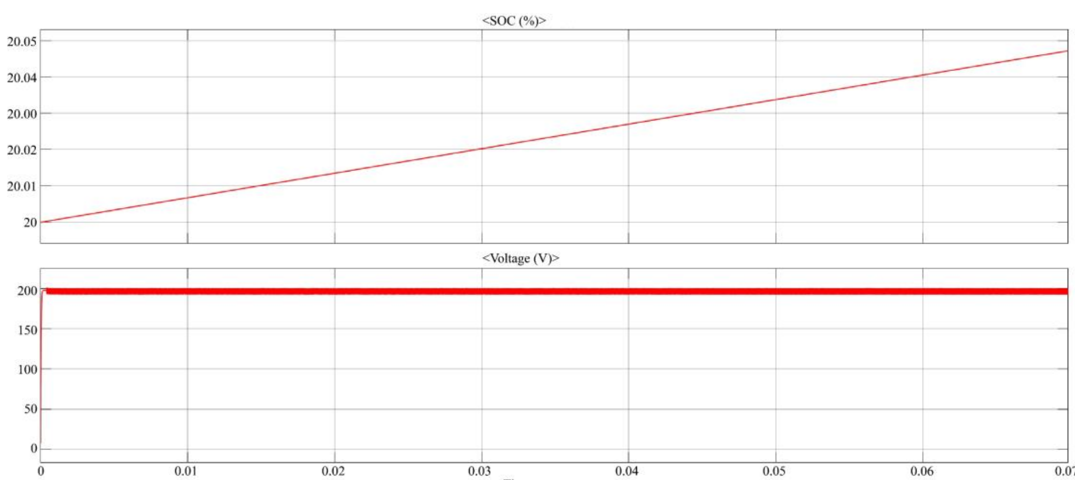

Fig. 10 Voltage and SOC during step up /boost mode in High-voltage (SU) battery side

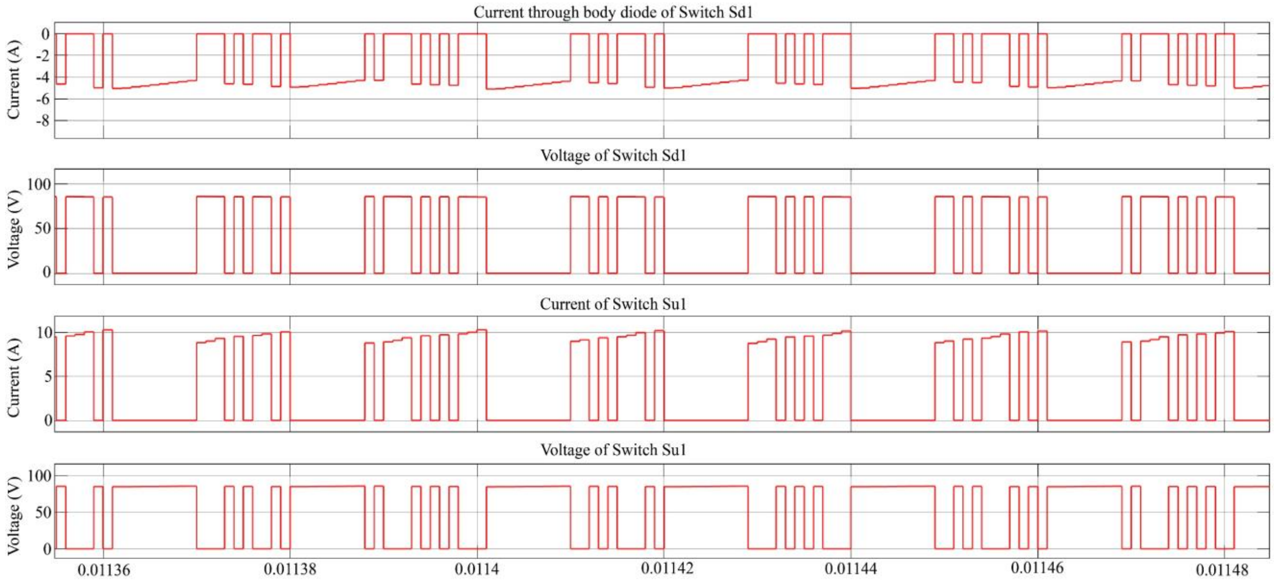

Fig. 11 Switching waveform of switches S_{d1} and S_{u1} during step up /Boost mode represents Voltage and current

5.1. Voltage Gain Characteristics

Figures 15 and 16 show a voltage gain comparison of the converter with several existing bidirectional DC-DC converters. These figures illustrate how the presented converter performs in terms of voltage gain.

In buck mode (Figure 15), competing designs [20] show the lowest voltage gain, but their usable operating range is limited due to the restricted voltage gain relationship given by ($D^2/(2+D)$).

These limitations restrict their voltage conversion range to 0-1/3, making them less versatile for practical applications. In contrast, the presented converter not only operates across a lowest broader range but also achieves lower minimum buck gains, providing enhanced operating flexibility.

Similarly, in boost mode (Figure 16), converter [20] exhibits a minimum gain of 3 due to its $(3-D)/(1-D)^2$ relationship, while in presented converter initiates gain from unity, ensuring smoother and wider scalability.

Other converters, such as those reported in [10, 12, 22, 24] with quadratic gain characteristics, provide comparable voltage gain capability; however, they offer limitations in terms of operating range, power-handling and over-performance trade-offs.

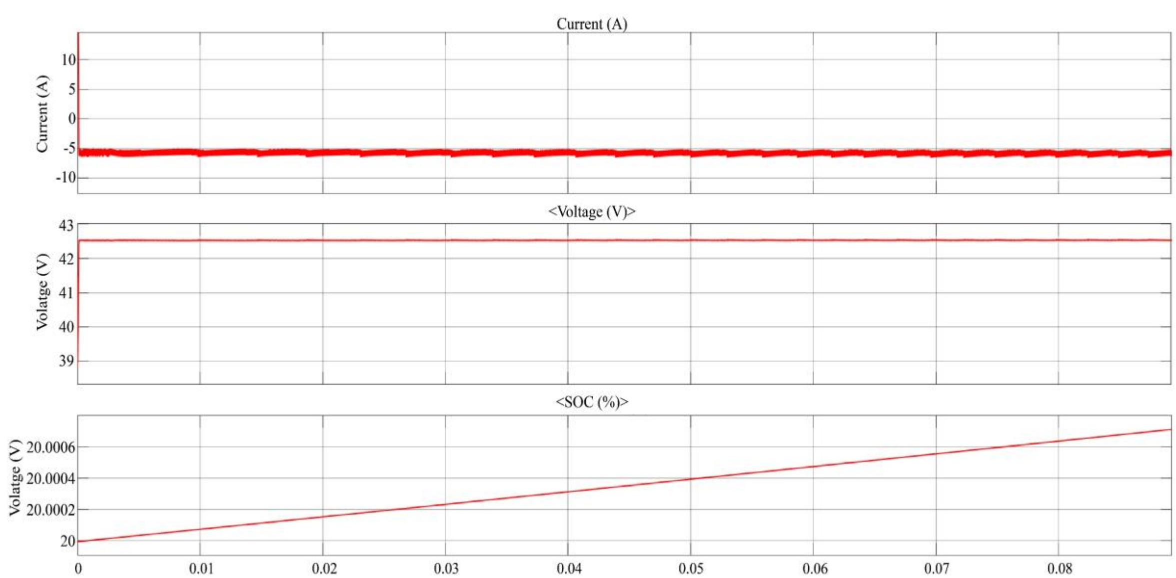

Fig. 12 Voltage, current, and SOC during step down /buck mode in Low-voltage (EV side) battery side

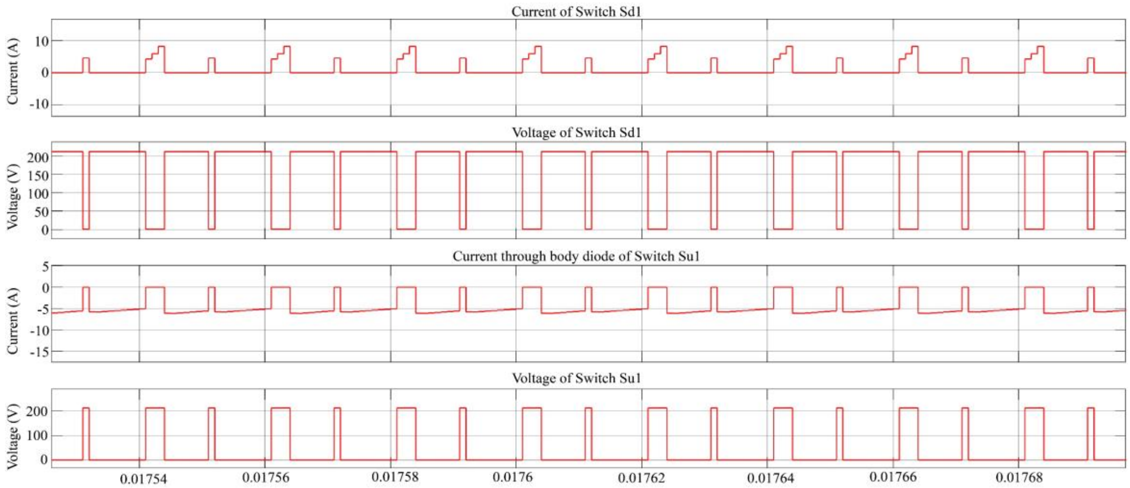

Fig. 13 Voltage and SOC during step down (buck) mode in High-voltage (SU) battery side

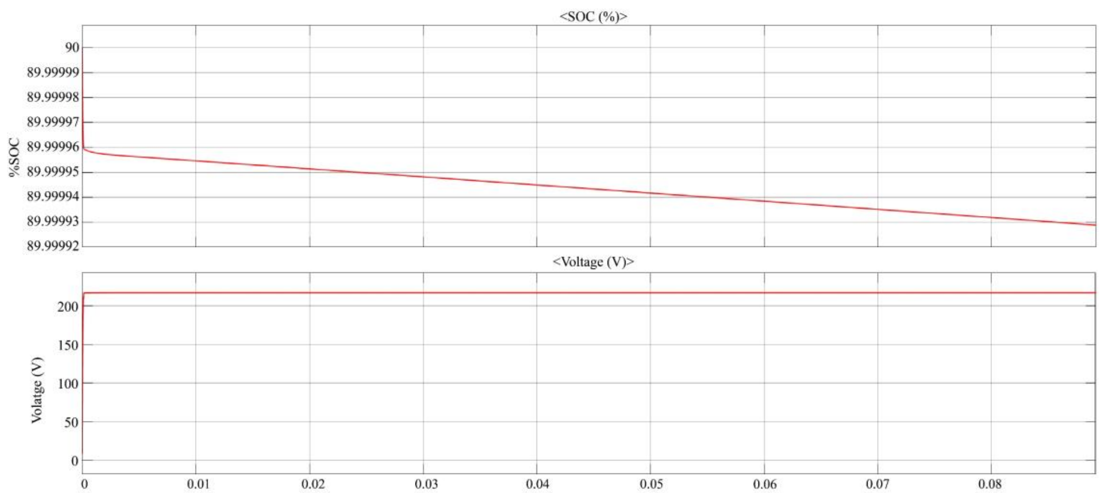

Fig. 14 Switching wave forms during step-down (buck) mode showing voltage across and current through switches S_{d1} and S_{u1}

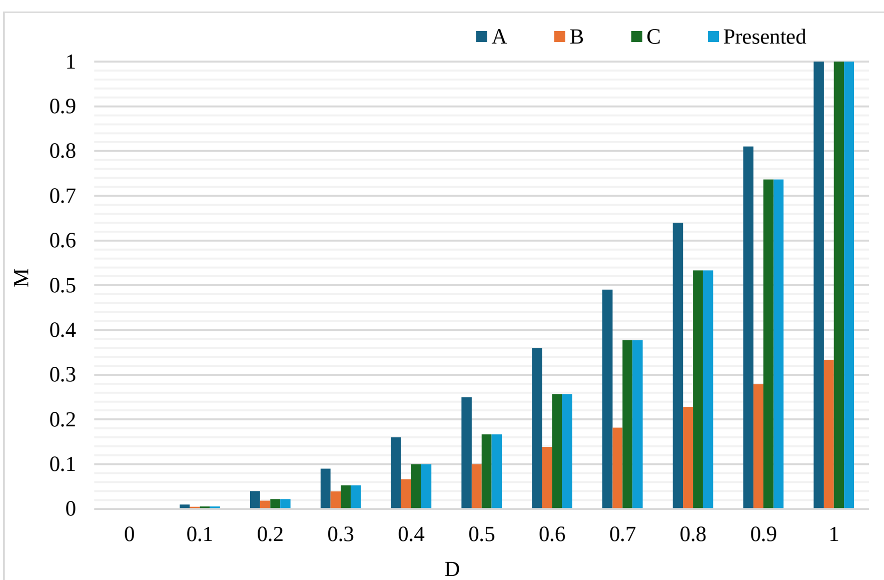

Fig. 15 Comparison of Voltage gain (M) for buck mode{Reference A-(11,13,25); B-(21); C-(23)}

5.2. Normalized voltage stress

In addition to gain performance, practical considerations such as voltage stress across switches and component utilization also matter significantly in converter evaluation. As shown in Figure 17, voltage stress across the semiconductor switches, normalized to the high-side voltage $(\Sigma V_{Sj} / V_{HV})$, is significantly lower in this design.

Although the stress data in [20] appears to offer slightly better stress figures, but does not operate in the critical gain range 1/3-1, making it less suitable for applications requiring operation within this voltage conversion range.

5.3. Semiconductor Utilization factor

Figure 18 shows the semiconductor utilization curve of other major compared converters with respect to voltage gain in terms of the Semiconductor Utilization Factor (SUF). The SUF is a crucial factor in converter design, as it directly impacts overall cost of the system. A higher SUF indicates more efficient utilization of semiconductor devices; consequently, it can lower overall system cost by minimizing the number of devices required or enabling the selection of devices with lower ratings. The SUF can be expressed as: SUF = $(P_O/\Sigma_j^k V_{Sj} I_{sj})$, where k denotes total number of semiconductor devices, I_{sj} and V_{Sj} is the maximum current and voltages of devices j, respectively. A higher SUF can reduce the voltage and current stress on semiconductor devices, leads to reliability. The presented Converter again performs remarkably well, providing higher utilization efficiency across the operating range compared to references [10, 12, 20, 22, 24].

5.4. Efficiency

The efficiency calculation involves the ratio of output power to the input power. Typically, a converter's efficiency increases with increasing output power due to reduced switching and conduction losses. However, efficiency may decrease at higher power levels, due to increased conduction losses, passive component losses and voltage drops across various components.

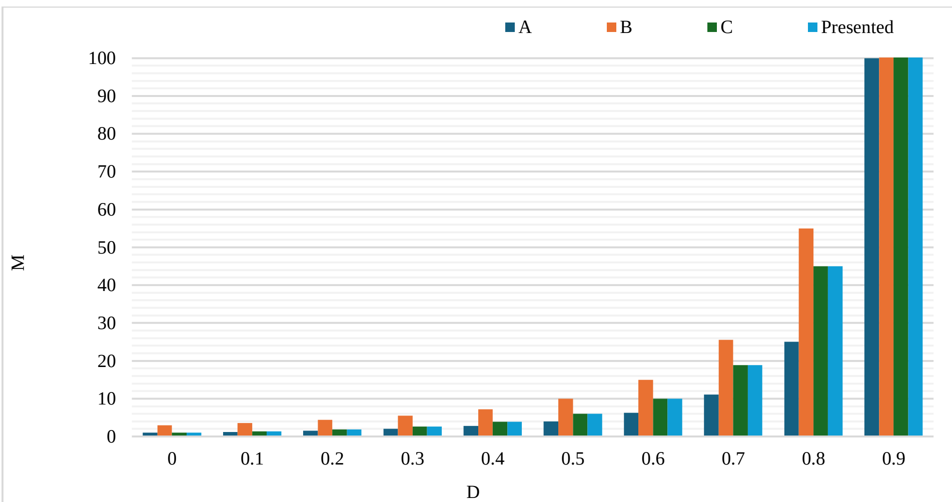

Fig. 16 Comparison of Voltage gain (M) for Boost Mode{Reference A-(11,13,25); B-(21); C-(23)}

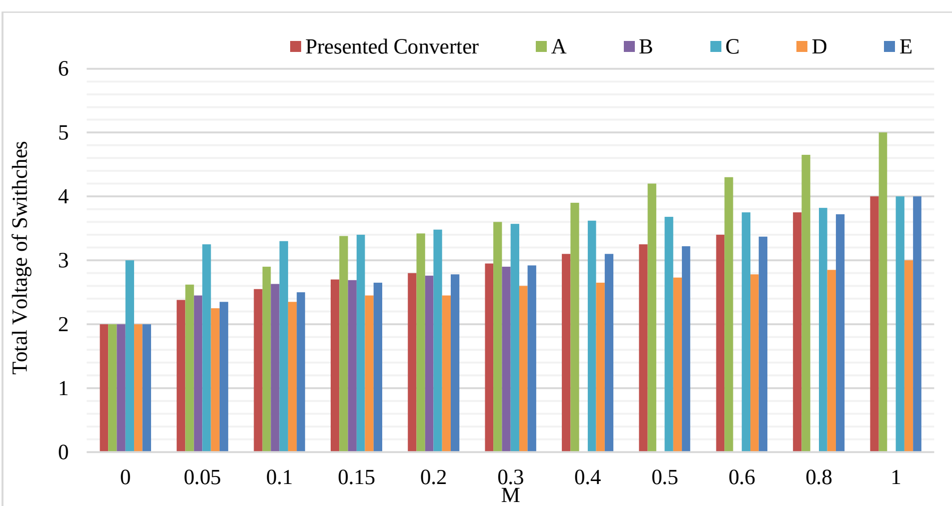

Fig. 17 Comparison of total voltage of Switches normalized w.r.t high voltage {A-(13); B-(21); C-(25); D (17); E-(23)}

SSRG International Journal of Electrical and Electronics Engineering
ISSN: 2348-8379/ https://doi.org/10.14445/23488379/IJEEE-V13I8P109

Volume 13 Issue 8, 99-113, August 2026

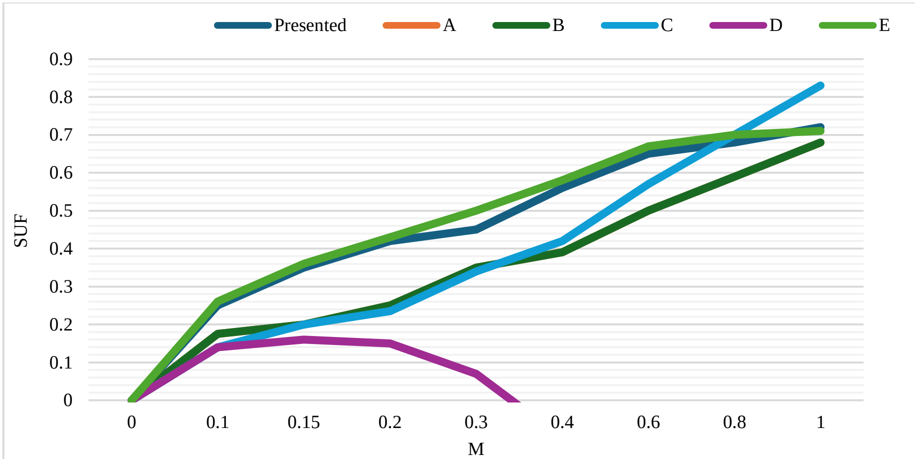

Fig. 18 Comparison of Semiconductor Utilization Factor (SUF) w.r.t Voltage Gain (M) for Buck Mode {Reference A-(17); B-(13); C-(25); D-(21); E-(23)}

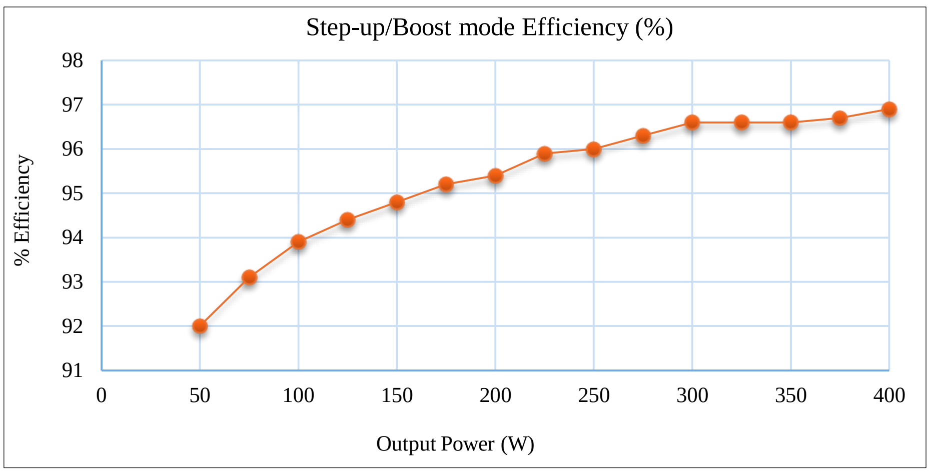

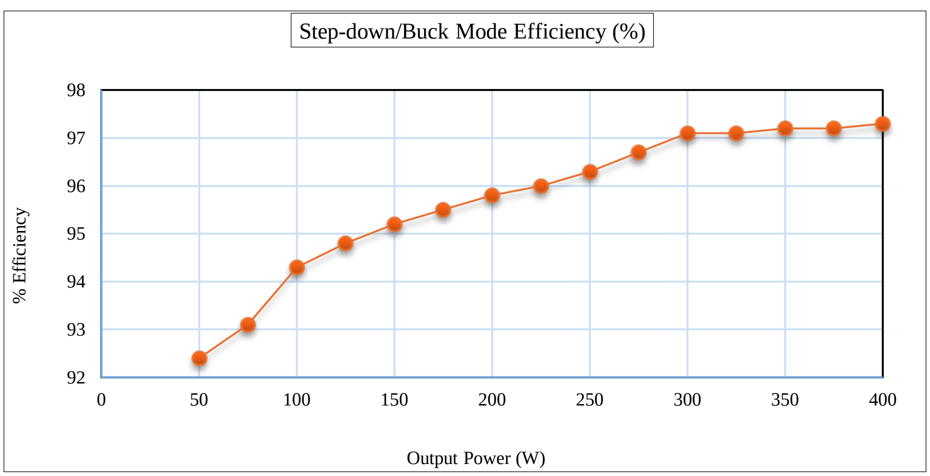

Fig. 19 Efficiency of the presented converter in both modes

Figure 19 presents the efficiency curve with respect to output power for the presented converter as a function of output power under both buck and boost modes. It is observed that the maximum efficiency of the converter is 97.3% and 96.9% in buck and boost modes, respectively. This efficiency shows the usability of the converter for demanding EV applications. While the work provides an analytical and simulation- based validation of the presented converter, the results indicate considerable potential performance for practical use in EV charging/discharge applications. It can be concluded that with its various features, such as wide voltage gain, lower semiconductor stress, consistently high efficiency and high

SUF, this converter is especially useful in applications requiring regular charging and discharging operations. The efficiency difference compared with [22] is affected by several factors, including operating conditions, power rating, implementation platform and the adopted control strategy. The lower power rating in the present work may contribute to reduced conduction losses due to lower current levels. In addition, the use of a PI controller introduces different control characteristics compared with the deadbeat controller employed in [22], which may affect the converter's dynamic response, switching pattern and related power losses. Consequently, the observed efficiency variation results from the combined influence of the converter operating conditions control strategy and implementation approach, and cannot be attributed to topology alone. The comparison of circuit complexity and application suitability of the bidirectional DC-DC converters presented in Table 3 clearly indicates that the adopted converter topology requires a reasonable number of components, offers better performance and overall application suitability as compared to many existing isolated or non-isolated topologies. In Table 3, the overall suitability rating of the converter indicates that the rating reflects the adopted topology rather than a new contribution, with its independent validation done as reported in the present study. This leads to more cost-effective and simpler design. The converter can maintain high efficiency, reduced stress on switching devices, as well as the reliability through its ability to manage the bi-directional of power flow. In addition, the topology allows for both V2G and G2V operations and indicates high suitability for Electric Vehicle (EV) applications due to its wide voltage gain range.

Table 3. Comparison of circuit complexity and application suitability of bidirectional DC-DC converters

Ref.	Topology	Comp. Used	Control Method	Soft-Switching ZVS/ZCS	Galvanic Isolation	On-Board Charging Facility	Overall EV Application Suitability
[27]	Interleaved Non isolated Buck-Boost	2C,2L,4S	Interleaved PWM	Partial (ZCS)	NP	P	Medium (good for low-voltage ESS)
[28]	CLLC Resonant Isolated Converter	4C,2L,8S	Variable Frequency	Both	P	P	Very High (preferred for high-power OBC)
[29]	Non-Isolated Cascaded Buck-Boost Converter	2C,2L,4S	Cascaded PWM	No	NP	P (Limited)	Low/Medium/High (losses, complex control)
[30]	Phase-Shifted Full-Bridge Bidirectional Converter	2C,1L,8S	Phase-Shift PWM	ZVS	P	P	High (Robust for high power EV charging)
[31]	Switched Capacitor Based Bidirectional DC-DC Converter	4C,1L,6S	Fixed-Frequency PWM	Partial (soft charge)	NP	P	Medium (Low Inductor count, moderate power)
[32]	Coupled Inductor High Step-Up Bidirectional Converter	2C,1L,4S	PWM + Duty Cycle Control	Partial (ZCS turn-off)	NP	P	High (Suits wide voltage range EV ESS)
[33]	Dual Active Bridge (DAB) Isolated Converter	2C,1L,8S	Phase-Shift Modulation	Both	P	P	High (Widely used in OBC design)
[34]	Multi-Level Bidirectional DC-DC Converter (3-Level)	3C,1L,6S	Multi-Level PWM	ZVS	P	P	High (Low ripple, Suited for high-Voltage EV Charging)
[22]	Non-Isolated Bidirectional Buck-Boost Converter	2C,4L,5S	PWM (Buck / Boost mode)	Both	NP	P	High (High eff, wide gain, low stress,500-W,40/200V)
Presented	High-Efficiency Non-Isolated Bidirectional Buck-Boost Converter	2C,4L,5S	PWM (Buck / Boost mode)	Both (reduced switch stress)	NP	P	High (validated at 400-W,48/200 V)

ESS: Energy Storage System; OBC: On-Board Charger; ZVS: Zero Voltage Switching; ZCS: Zero Current Switching; Component Used-C: Capacitor, L: Inductor, S: Switch, P: Present, NP: Not Present

6. Conclusion

The paper presented the MATLAB/Simulink implementation and performance evaluation of a converter allowing energy flow in either direction depending on requirement for EV charging applications. The converter was evaluated for a 400-W system with a 48 V/200 V operating configuration. Based on the analysis and performance evaluation, the following conclusions can be drawn:

1. The MATLAB/Simulink implementation successfully demonstrates stable bidirectional power transfer in both buck and boost operating modes, validating the applicability of the adopted converter topology under the selected operating conditions.
2. Results are in close agreement with the theoretical analysis. The maximum efficiency of the converter is 97.3% in buck mode, and 96.9% in boost mode are observed, indicating strong performance compared to a conventional design.
3. The performance evaluation verifies that the adopted converter demonstrates competitive efficiency and voltage gain capabilities while maintaining moderate component count and reduced normalized semiconductor stress, factors important for the practical application of EV energy transfer systems.

Overall, the presented implementation and analysis demonstrate that the adopted bidirectional converter topology can provide reliable and efficient operation for EV charging and V2G applications while serving as a useful reference model for further research and development.

6.1. Future Scope

1. Development of experimental prototypes involving thermal analysis, controller implementation and efficiency evaluation for hardware elements is currently underway and will be documented in future works.
2. AI-driven Optimization: The effective charging schedule can be developed by considering the analysis of user behaviours, variation in charging demand, grid limitations and weather conditions.
3. Future scope may available for thermal stress analysis, dynamic load response.

Acknowledgements

The Authors thank Integral University, Lucknow, for academic support and providing Manuscript Communication Number IU/R&D/2026-MCN0004701.

Author contributions

All authors have equally contributed in writing, editing, and revision work, and all approved the final manuscript.

Data availability

The authors confirm that all the data analyzed during this study are available in the article.

Conflict of interest

The authors declare that there is no competing interest related to this study.

References

[1] Francis Mwasilu et al., “Electric Vehicles and Smart Grid Interaction: A Review on Vehicle to Grid and Renewable Energy Sources Integration,” *Renewable and Sustainable Energy Reviews*, vol. 34, pp. 501-516, 2014. [CrossRef] [Google Scholar] [Publisher Link]

[2] Sithara S.G. Acharige et al., “Review of Electric Vehicle Charging Technologies, Standards, Architectures, and Converter Configurations,” *IEEE Access*, vol. 11, pp. 41218-41255, 2023. [CrossRef] [Google Scholar] [Publisher Link]

[3] Shemin Sagaria, Mart van der Kam, and Tobias Boström, “Vehicle-to-Grid Impact on Battery Degradation and Estimation of V2G Economic Compensation,” *Applied Energy*, vol. 377, pp. 1-21, 2025. [CrossRef] [Google Scholar] [Publisher Link]

[4] Marif Daula Siddique et al., “A New Configurable Switched-Capacitor based Boost Inverter with Reduced Component Count for Renewable Energy Applications,” *e-Prime - Advances in Electrical Engineering, Electronics and Energy*, vol. 9, pp. 1-19, 2024. [CrossRef] [Google Scholar] [Publisher Link]

[5] Akhlaque Ahmad Khan et al., “Optimal Sizing, Control, and Management Strategies for Hybrid Renewable Energy Systems: A Comprehensive Review,” *Energies*, vol. 15, no. 17, pp. 1-29, 2022. [CrossRef] [Google Scholar] [Publisher Link]

[6] Mohammad Aslam Alam, Ahmad Faiz Minai, and Farhad Ilahi Bakhsh, “Isolated Bidirectional DC-DC Converter: A Topological Review,” *e-Prime - Advances in Electrical Engineering, Electronics and Energy*, vol. 8, pp. 1-19, 2024. [CrossRef] [Google Scholar] [Publisher Link]

[7] Nour Elsayad, Hadi Moradisizkoohi, and Osama A. Mohammed, “Design and Implementation of a New Transformerless Bidirectional DC-DC Converter with Wide Conversion Ratios,” *IEEE Transactions on Industrial Electronics*, vol. 66, no. 9, pp. 7067-7077, 2018. [CrossRef] [Google Scholar] [Publisher Link]

[8] Yun Zhang et al., “A Switched-Capacitor Interleaved Bidirectional Converter with Wide Voltage-Gain Range for Super Capacitors in Evs,” *IEEE Transactions on Power Electronics*, vol. 35, no. 2, pp. 1536-1547, 2019. [CrossRef] [Google Scholar] [Publisher Link]

[9] Bader N. Alajmi et al., “Phase Shift Full Bridge DC-DC Converter with Active Clamping Circuit for Fuel Cell Electric Vehicles,” *IEEE Access*, vol. 13, pp. 90875 - 90895, 2025. [CrossRef] [Google Scholar] [Publisher Link]

[10] Hossein Ardi, Rouzbeh Reza Ahrabi, and Sajad Najafi Ravadanegh, “Non-Isolated Bidirectional DC-DC Converter Analysis and Implementation, *IET Power Electronics*, vol. 7, no. 12, pp. 3033-3044, 2014. [CrossRef] [Google Scholar] [Publisher Link]

[11] K.S. Kavin et al., “Improved BRBFNN-based MPPT Algorithm for Coupled Inductor KSK Converter for Sustainable PV System Applications,” *Electrical Engineering*, vol. 107, no. 6, pp. 7831-7853, 2025. [CrossRef] [Google Scholar] [Publisher Link]

[12] Hossein Ardi et al., “Analysis and Implementation of a Nonisolated Bidirectional DC-DC Converter with High Voltage Gain,” *IEEE Transactions on Industrial Electronics*, vol. 63, no. 8, pp. 4878-4888, 2016. [CrossRef] [Google Scholar] [Publisher Link]

[13] Shilpa Ghode, and Mayuri Digalwar, "Enhanced Electric Vehicle Charging Strategy through Graph Convolutional Networks Integrated with Deep Reinforcement Learning," *International Journal of Information Technology*, vol. 17, no. 7, pp. 4217-4229, 2025. [CrossRef] [Google Scholar] [Publisher Link]

[14] Krishna Mainali, and Ramesh Oruganti, "Conducted EMI Mitigation Techniques for Switch-Mode Power Converters: A Survey," *IEEE Transactions on Power Electronics*, vol. 25, no. 9, pp. 2344-2356, 2010. [CrossRef] [Google Scholar] [Publisher Link]

[15] C.-C. Lin, L.-S. Yang, and G.W. Wu, "Study of a Non-Isolated Bidirectional DC-DC Converter," *IET Power Electronics*, vol. 6, no. 1, pp. 30-37, 2013. [CrossRef] [Google Scholar] [Publisher Link]

[16] Daniel Flores Cortez et al., "DC-DC Converter for Dual-Voltage Automotive Systems based on Bidirectional Hybrid Switched-Capacitor Architectures," *IEEE Transactions on Industrial Electronics*, vol. 62, no. 5, 2015. [CrossRef] [Google Scholar] [Publisher Link]

[17] Yun Zhang et al., "Hybrid Switched-Capacitor/Switched-Quasi-Z-Source Bidirectional DC-DC Converter with a Wide Voltage Gain Range for Hybrid Energy Sources Evs," *IEEE Transactions on Industrial Electronics*, vol. 66, no. 4, pp. 2680-2690, 2019. [CrossRef] [Google Scholar] [Publisher Link]

[18] Hyeonju Jeong, Minho Kwon, and Sewan Choi, "Analysis, Design, and Implementation of a High Gain Soft-Switching Bidirectional DC-DC Converter with PPS Control," *IEEE Transactions on Power Electronics*, vol. 33, no. 6, pp. 4807-4816, 2018. [CrossRef] [Google Scholar] [Publisher Link]

[19] Yun Zhang et al., "A Switched-Capacitor Bidirectional DC-DC Converter with Wide Voltage Gain Range for Electric Vehicles with Hybrid Energy Sources," *IEEE Transactions on Power Electronics*, vol. 33, no. 11, pp. 9459-9469, 2018. [CrossRef] [Google Scholar] [Publisher Link]

[20] Nour Elsayad, Hadi Moradisizkoohi, and Osama A. Mohammed, "A New Hybrid Structure of a Bidirectional DC-DC Converter with High Conversion Ratios for Electric Vehicles," *IEEE Transactions on Vehicular Technology*, vol. 69, no. 1, pp. 194-206, 2020. [CrossRef] [Google Scholar] [Publisher Link]

[21] Sara Mousavinezhad Fardahar, and Mehran Sabahi, "New Expandable Switched-Capacitor/Switched-Inductor High-Voltage Conversion Ratio Bidirectional DC-DC Converter," *IEEE Transactions on Power Electronics*, vol. 35, no. 3, pp. 2480-2487, 2020. [CrossRef] [Google Scholar] [Publisher Link]

[22] Hamed Heydari-doostabad, and Terence O'Donnell, "A Wide-Range High-Voltage-Gain Bidirectional DC-DC Converter for V2G and G2V Hybrid EV Charger," *IEEE Transactions on Industrial Electronics*, vol. 69, no. 5, pp. 4718-4729, 2022. [CrossRef] [Google Scholar] [Publisher Link]

[23] Jianliang Chen et al., "Cascaded High Voltage Conversion Ratio Bidirectional Nonisolated DC-DC Converter with Variable Switching Frequency," *IEEE Transactions on Power Electronics*, vol. 33, no. 2, pp. 1399-1409, 2017. [CrossRef] [Google Scholar] [Publisher Link]

[24] Vitor Fernão Pires, Daniel Foito, and Armando Cordeiro, "A DC-DC Converter with Quadratic Gain and Bidirectional Capability for Batteries/Supercapacitors," *IEEE Transactions on Industry Applications*, vol. 54, no. 1, pp. 274-285, 2017. [CrossRef] [Google Scholar] [Publisher Link]

[25] Ke Jin et al., "Three-Level Bidirectional Converter for Fuel-Cell/Battery Hybrid Power System," *IEEE Transactions on Industrial Electronics*, vol. 57, no. 6, pp. 1976-1986, 2010. [CrossRef] [Google Scholar] [Publisher Link]

[26] Lung-Sheng Yang, and Tsorng-Juu Liang, "Analysis and Implementation of a Novel Bidirectional DC-DC Converter," *IEEE Transactions on Industrial Electronics*, vol. 59, no. 1, pp. 422-434, 2011. [CrossRef] [Google Scholar] [Publisher Link]

[27] Stefan Waffler, and Johann W. Kolar, "A Novel Low-Loss Modulation Strategy for High-Power Bidirectional Buck+Boost Converters," *IEEE Transactions on Power Electronics*, vol. 24, no. 6, pp. 1589-1599, 2009. [CrossRef] [Google Scholar] [Publisher Link]

[28] Zaka Ullah Zahid et al., "Design of Bidirectional DC-DC Resonant Converter for Vehicle-to-Grid (V2G) Applications," *IEEE Transactions on Transportation Electrification*, vol. 1, no. 3, pp. 232-244, 2015. [CrossRef] [Google Scholar] [Publisher Link]

[29] Mamadou Baiio Camara et al., "DC/DC Converter Design for Supercapacitor and Battery Power Management in Hybrid Vehicle Applications-Polynomial Control Strategy," *IEEE Transactions on Industrial Electronic*s, vol. 57, no. 2, pp. 587-597, 2010. [CrossRef] [Google Scholar] [Publisher Link]

[30] In-Dong Kim et al., "New Bidirectional ZVS PWM Sepic/Zeta DC-DC Converter," *2007 IEEE International Symposium on Industrial Electronics*, Vigo, Spain, pp. 555-560, 2007. [CrossRef] [Google Scholar] [Publisher Link]

[31] Lung-Sheng Yang et al., "Novel High Step-up DC-DC Converter with Coupled-Inductor and Voltage-Doubler Circuits," *IEEE Transactions on Industrial Electronics*, vol. 58, no. 9, pp. 4196-4206, 2011. [CrossRef] [Google Scholar] [Publisher Link]

[32] Hui Li, Fang Zheng Peng, and J.S. Lawler, "A Natural ZVS Medium-Power Bidirectional DC-DC Converter with Minimum Number of Devices," *IEEE Transactions on Industry Applications*, vol. 39, no. 2, pp. 525-535, 2003. [CrossRef] [Google Scholar] [Publisher Link]

[33] R.W.A.A. De Doncker, D.M. Divan, and M.H. Kheraluwala, "A Three-Phase Soft-Switched High-Power-Density DC/DC Converter for High-Power Applications," *IEEE Transactions on Industry Applications*, vol. 27, no. 1, pp. 63-73, 1991. [CrossRef] [Google Scholar] [Publisher Link]

[34] F.Z. Peng, and Fan Zhang, "A Novel Compact DC/DC Converter for 42 V Systems," *Power Electronics in Transportation*, Auburn Hills, MI, USA, pp. 143-148, 2002. [CrossRef] [Google Scholar] [Publisher Link]